The *E. Coli* Replication Factor DnaC Protein Exists in Two Conformations with Different Nucleotide Binding Capabilities. I. Determination of the Binding Mechanism Using ATP and ADP Fluorescent Analogues†

Roberto Galletto and Wlodzimierz Bujalowski*

Department of Human Biological Chemistry & Genetics and The Sealy Center for Structural Biology, The University of Texas Medical Branch at Galveston, Galveston, Texas 77555-1053

Received February 12, 2002; Revised Manuscript Received April 8, 2002

ABSTRACT: The kinetic mechanism of binding of ATP and ADP fluorescent analogues to the *E. coli* replicative factor DnaC protein has been studied using the fluorescence stopped-flow technique. The experiments have been performed under pseudo-first-order conditions with respect to the nucleotide cofactor or the DnaC concentration. Three relaxation processes are observed at a large excess of the nucleotide, while only two relaxation processes are detected in the excess of the protein. Such behavior of the kinetic system is a diagnostic indication of the presence of the protein conformational equilibrium prior to the ligand binding. The obtained data indicate that the minimum mechanism that describes the observed kinetics includes the conformational transition of the DnaC protein, prior to nucleotide binding, followed by the two-step, sequential association of the cofactor to only one of the protein conformations, as defined by

$$(\mathrm{DnaC})_1 \underset{k_{-1}}{\overset{k_1}{\rightleftarrows}} (\mathrm{DnaC})_2$$

$$\mathrm{Nucleotide} + (\mathrm{DnaC})_2 \underset{k_{-2}}{\overset{k_2}{\rightleftarrows}} (\mathrm{C})_1 \underset{k_{-3}}{\overset{k_3}{\rightleftarrows}} (\mathrm{C})_2$$

In the examined solution conditions, the conformation of the DnaC protein is shifted toward the state $(\mathrm{DnaC})_2$ that binds the nucleotide. The lack of any cofactor binding to the $(\mathrm{DnaC})_1$ state points to the existence of a stringent locking mechanism of the nucleotide binding-site in the protein. Binding of ATP and ADP analogues obeys the same mechanism, with similar rate constants, indicating that ATP and ADP analogues bind to the same protein conformation. The $(\mathrm{C})_1$ intermediate dominates the distribution of the DnaC protein population in the presence of cofactors. The formation of $(\mathrm{C})_1$ is accompanied by a low nucleotide fluorescence increase, indicating a hydrophilic environment around the ribose of bound cofactors. Transition to $(\mathrm{C})_2$ places the ribose region in a highly hydrophobic environment with relative molar fluorescence intensity ∼8-fold higher than that of the free cofactor. The significance of these results for the functioning of the DnaC protein is discussed.

The DnaC protein is an essential replication protein in the *Escherichia coli* cell (*1*−*5*). Both fast- and slow-stop mutations of the protein have been identified, indicating that the protein is involved in initiation and elongation stages of the chromosomal DNA replication, as well as in the replication of phage and plasmid DNAs (*1*−*7*). The DnaC protein participates in the formation of the replication fork as well as in the assembly of the primosome, a multi-protein−DNA complex which can translocate along the DNA while synthesizing short oligoribonucleotide primers that are used to initiate synthesis of the complementary strand (*1*, *2*, *8*). In these capacities, the DnaC protein is thought to specifically interact, in the presence of ATP, with the *E. coli* primary replicative helicase, the DnaB protein, allowing the helicase to recognize specific protein−DNA complexes, most probably through interactions with other replication proteins (*1*, *9*−*15*).

The DnaC protein is not necessary for the DnaB helicase to bind the ssDNA. The helicase can form a complex with the nucleic acid with significant affinity without DnaC (*16*−*21*). Rather, the binding of DnaC to the DnaB protein allows the helicase to recognize the protein−nucleic acid complex formed at the replication origin (oriC) (*1*, *9*, *10*). The DnaC protein is absolutely required for this reaction. In the formation of the primosome, the DnaC−DnaB complex allows the helicase to recognize a specific multi-protein−DNA complex, which includes PriA, PriB, PriC, and DnaT proteins at the primosome assembly site (PAS) (*8*, *15*). Due

† This work was supported by NIH Grant GM-46679 (to W. B.).

* Corresponding author. Tel: (409) 772-5643. Fax: (409) 772−1790. E-mail: wbujalow@utmb.edu.

[1] Abbreviations: MANT-ATP, 3′-O-(*N*-methylantraniloyl)-5′-triphosphate; MANT-ADP, 3′-O-(*N*-methylantraniloyl)-5′-diphosphate; Tris, tris(hydroxymethyl)aminomethane; DTT, dithiothreitol.

10.1021/bi0201264 CCC: $22.00
Published on Web 06/19/2002

to its highly specific role in "delivering" the replicative helicase to specific replication complexes and the ATP requirement for these reactions, the DnaC protein has been termed the "molecular matchmaker" (*22*).

Current views on the role of the DnaC protein in DNA replication strictly relate it to the highly specific interactions of the protein with the *E. coli* primary replicative helicase, the DnaB protein, which are under ATP control (*1*−*5*, *9*, *10*, *24*−*26*). In contrast, ADP was proposed not to support these interactions. However, the hydrolysis of ATP is not necessary for the complex formation, although this has not been rigorously proven. The DnaC protein does not have intrinsic ATPase activity. These results suggest that ATP acts as a positive effector, inducing conformational changes in the DnaC protein and increasing its affinity for the helicase, while ADP acts as a negative effector.

Recent thermodynamic studies, using fluorescent nucleotide analogues and unmodified nucleotides, have provided the first insight into the energetics of the DnaC protein interactions with nucleotide cofactors (*27*). The DnaC protein has a single nucleotide-binding site. The site is highly specific for the adenine base. Binding of nucleotides containing bases different than adenine has not been detected. However, the structure of the triphosphate group and the 2′ hydroxyl group of the ribose play important roles in the stabilization of the formed complex. The most surprising result is that both ATP and ADP have the same affinity for the nucleotide-binding site of the DnaC protein yet only ATP is proposed to induce a high-affinity state for the binding to the DnaB helicase (*9*, *10*). These data clearly indicate that the efficient association of the nucleotides with the DnaC protein is not enough to trigger specific conformational changes of the entire protein, leading to an increased affinity toward the DnaB helicase.

Elucidation of nucleotide interactions with the DnaC protein and their regulatory role is of paramount importance for our understanding of the activities of this essential replication factor. In this communication, we quantitatively examine the kinetic mechanism of the interactions of nucleotide cofactors with the DnaC protein using the fluorescent nucleotide analogues MANT-ATP and MANT-ADP. We provide direct evidence that the DnaC protein exists in a pre-equilibrium conformational transition prior to the nucleotide binding. The nucleotide cofactor binds to only one of the protein conformations. Moreover, both MANT-ATP and MANT-ADP bind to the same protein conformation in a two-step sequential process in which the bimolecular reaction is followed by a single conformational transition of the formed protein−nucleotide complex.

MATERIALS AND METHODS

Reagents and Buffers. All chemicals were reagent grade. All solutions were made with distilled and deionized 18 MΩ (Milli-Q) water. The standard buffer, T4, is 50 mM Tris adjusted to pH 8.1 at the appropriate temperature with HCl, 5 mM $MgCl_2$, 10% glycerol, and 1 mM DTT. The salt concentration in the buffer is indicated in the text.

Nucleotides. MANT-ATP and MANT-ADP were synthesized as previously described (*28*−*30*). Fluorescent nucleotide analogues used in the studies were >95% pure, as judged by TLC on silica. The concentrations of the nucleotides were determined using the extinction coefficient $\epsilon_{356} = 5800\ M^{-1}\ cm^{-1}$.

DnaC Protein. The *E. coli* DnaC protein was purified as previously described by us (*27*). The concentration of the protein was spectrophotometrically determined using the extinction coefficient $\epsilon_{280} = 23.2 \times 10^4\ M^{-1}\ cm^{-1}$ (*27*).

Stopped-Flow Kinetics. All fluorescence stopped-flow kinetics experiments were performed using the SX.18MV stopped-flow instrument (Applied Photophysics, Leatherhead, UK) equipped with the FP.1 fluorescence polarization/anisotropy accessory. The FP.1 dual channel, T-format fluorescence polarimeter allows the direct determination of the fluorescence total emission, $I_{VV} = I_{VV} + 2I_{VH}$, avoiding any bias of the signal which might originate from changing the degree of fluorescence polarization of the sample during the reaction (*34*, *35*). The reactions were monitored following the fluorescence emission of the MANT group, with $\lambda_{ex} =$ 356 nm, and the emission was monitored through the GG400 cutoff filter (Schott, PA). The excitation monochromator slits were at 1.5 mm (band-pass ≈ 7 nm). The experiments were performed in the "oversampling" mode (*36*,*37*). Four to twelve traces were collected and averaged for each sample. The relaxation times and amplitudes for each kinetic trace were determined using the nonlinear, least-squares software provide by the manufacturer, with the exponential function defined as

$$F(t) = F(\infty) + \sum_{i=1}^{n} A_i \exp(-\lambda_i t) \qquad (1)$$

where $F(t)$ is the fluorescence intensity at time t, $F(\infty)$ is the fluorescence intensity at time $t = \infty$, A_i is the amplitude corresponding to the ith relaxation process, λ_i is the time constant (reciprocal relaxation time) characterizing the ith relaxation process, and n is the number of relaxation processes. All further analyses of the data were performed using Mathematica (Wolfram, Urbana, IL) and KaleidaGraph (Synergy Software, PA) on MacIntosh G4 computers.

THEORY

Pre-equilibrium Conformational Transition of the Macromolecule Prior to the Ligand Binding versus Sequential Binding Mechanism. Kinetic methods are the most sensitive techniques for detecting the presence of any conformational transition of the macromolecule prior to the ligand binding (*38*−*42*). Such detection is based on the fact that under pseudo-first-order conditions with respect to the ligand concentration, the reciprocal relaxation time characterizing the conformational transition will decrease with the increasing ligand concentration (*38*−*40*). The sequential mechanism with the same number of elementary steps cannot generate analogous behavior (*38*−*40*). The underlying assumption of the approach is that all relaxation processes are decoupled, i.e., they are well separated on the time scale of the reaction. However, in a general situation, this may not be the case. If the experiments are performed only under pseudo-first-order conditions with respect to the ligand concentration, the pre-equilibrium mechanism may be very difficult to distinguish from the sequential one with the same number of elementary steps, both in the behavior of the relaxation times and in the amplitudes of the reaction. On the other hand, the combined application of pseudo-first-order conditions of both ligand and macromolecule concentrations will allow the experi-

menter to distinguish these fundamentally different kinetic mechanisms (*36*−*41*).

The kinetic data described in this work indicate that the DnaC protein exists in two conformations prior to the nucleotide cofactor binding and that the nucleotide binds only to one conformation of the protein. As an example, we consider binding of the fluorescent ligand, N, to the macromolecule, P, where the macromolecule exists in two different conformations prior to the ligand binding. The ligand binds to only one conformation of the macromolecule in a sequential, two-step process. The considered mechanism is defined by eq 2:

$$\begin{gathered} P_1 \underset{k_{-1}}{\overset{k_1}{\rightleftarrows}} P_2 \\ N_1 + P_2 \underset{k_{-2}}{\overset{k_2}{\rightleftarrows}} P_3 \underset{k_{-3}}{\overset{k_3}{\rightleftarrows}} P_4 \end{gathered} \tag{2}$$

The reaction is monitored by the fluorescence changes of the ligand.

In our analysis, we use the matrix projection operator technique, which is a very powerful method of analyzing complex kinetics (*36*, *37*, *43*−*46*). The kinetic studies are performed under pseudo-first-order conditions with respect to the [ligand], i.e., in the large excess of the ligand, $[N]_{Tot} \gg [P]_{Tot}$. Thus, $[N_1]$ is approximately constant during the reaction. The system of differential equations, with respect to the macromolecular species, describing the time course of the reaction (eq 2) in matrix notation is defined as

$$\begin{pmatrix} \dot{P}_1 \\ \dot{P}_2 \\ \dot{P}_3 \\ \dot{P}_4 \end{pmatrix} = \begin{pmatrix} -k_1 & k_{-1} & 0 & 0 \\ k_1 & -(k_{-1}+k_2)[N_1] & k_{-2} & 0 \\ 0 & k_2[N_1] & -(k_{-2}+k_3) & k_{-3} \\ 0 & 0 & k_3 & -k_{-3} \end{pmatrix} \begin{pmatrix} P_1 \\ P_2 \\ P_3 \\ P_4 \end{pmatrix} \tag{3}$$

and

$$\dot{\mathbf{P}} = \mathbf{M_1 P} \tag{4}$$

where $\dot{\mathbf{P}}$ is the vector of time derivatives, $\mathbf{M_1}$ is the coefficient matrix, and $\mathbf{P}$ is the vector of concentrations of all macromolecule species. Using the matrix projection operators, the solution for the system of differential equations, defined by eq 3, is (*36*, *37*, *44*, *45*)

$$\mathbf{P} = \mathbf{Q_0 P_0} + \mathbf{Q_1 P_0} \exp(\lambda_1 t) + \mathbf{Q_2 P_0} \exp(\lambda_2 t) + \mathbf{Q_3 P_0} \exp(\lambda_3 t) \tag{5}$$

Thus, there are three normal modes of the examined reaction (eq 2). The quantities λ_1, λ_2, and λ_3 are eigenvalues of the coefficient matrix $\mathbf{M_1}$, $\mathbf{P_0}$ is the column vector of the initial concentrations of the macromolecule species, and $\mathbf{Q_i}$'s are the matrix projection operators (*36*, *37*, *44*).

At the time $t = 0$ of the reaction, the concentration of the total macromolecule is equal to the sum of the initial concentrations of P_1 and P_2, while the concentrations of all other macromolecule species are zero. Prior to the nucleotide binding, the concentrations of the macromolecular states are $P_1 = P_{Tot}/(1 + K_1)$ and $P_2 = P_{Tot}K_1/(1 + K_1)$, respectively, where K_1 is the equilibrium constant for the conformational transition of the macromolecule, i.e., $K_1 = k_1/k_{-1}$. The column vector $\mathbf{P_0}$ of the initial macromolecular species concentrations is then

$$\mathbf{P_0} = \begin{pmatrix} \dfrac{P_{Tot}}{1+K_1} & \dfrac{P_{Tot}K_1}{1+K_1} & 0 & 0 \end{pmatrix} \tag{6}$$

The three normal modes of reaction are characterized by relaxation times, τ_1, τ_2, and τ_3, described by the identities, $\tau_1 = -1/\lambda_1$, $\tau_2 = -1/\lambda_2$, and $\tau_3 = -1/\lambda_3$. The closed-form expressions for the three corresponding amplitudes, A_1, A_2, and A_3 are defined using the matrix projection operators in Appendix 1.

Under pseudo-first-order conditions with respect to the ligand concentration, the examination of the relaxation times as a function of the ligand concentration is the first and fundamental step in establishing the mechanism of a complex reaction (*36*−*41*). The reciprocal relaxation times for the reaction, described by eq 2, as a function of the free ligand concentration, are shown in Figure 1a−c. Relaxation times have been obtained by direct, numerical determination of the eigenvalues, λ_1, λ_2, and λ_3 of the matrix $\mathbf{M_1}$ at a given free ligand concentration. The selected rate constants are $k_1 = 7\ s^{-1}$, $k_{-1} = 6\ s^{-1}$, $k_2 = 1 \times 10^6\ M^{-1}\ s^{-1}$, $k_{-2} = 10\ s^{-1}$, $k_3 = 0.05\ s^{-1}$, and $k_{-3} = 0.01\ s^{-1}$. Thus, the rate constants differ to the extent that all three normal modes of the reaction are virtually decoupled (*38*).

The largest reciprocal of relaxation time, $1/\tau_1$, increases linearly with the [ligand] in the high ligand concentration range. This is typical behavior for the relaxation time characterizing the bimolecular binding process *(36*−*41)*. The reciprocal relaxation time, $1/\tau_2$, for the reaction described by eq 2 has its highest values at low ligand concentrations and decreases with the increasing [ligand]. Such functional dependence of any of the relaxation times of the examined reaction presents strong evidence of the existence of a preequilibrium conformational transition of the macromolecule prior to the ligand binding because a sequential reaction cannot generate such behavior *(36*−*41)*. The relaxation time $1/\tau_3$ shows characteristic, hyperbolic dependence upon the [ligand] and reaches plateau values at a higher [ligand], an indication that it characterizes an intramolecular transition as defined by eq 2.

However, the situation is very different if the rate constants for the partial steps of the reaction have similar values resulting in similar values of the relaxation times, at least in some range of the ligand concentration. The reciprocal relaxation times for the same reaction, described by eq 2, as functions of the free ligand concentration, are included in Figure 1a−c (dashed lines). The selected rate constants are $k_1 = 7\ s^{-1}$, $k_{-1} = 6\ s^{-1}$, $k_2 = 1 \times 10^6\ M^{-1}\ s^{-1}$, $k_{-2} = 3\ s^{-1}$, $k_3 = 0.05\ s^{-1}$, and $k_{-3} = 0.01\ s^{-1}$. Thus, the value of the rate constant, k_{-2}, is lower than the values of the rate constants characterizing the conformational transition of the macromolecule. Although the plot of $1/\tau_1$ is shifted down for lower values of k_{-2}, the behavior of $1/\tau_1$, as a function of the ligand concentration, is unchanged, an indication that the relaxation time characterizes the bimolecular binding process. On the other hand, the behavior of the reciprocal relaxation time, $1/\tau_2$, is dramatically changed. The plot shows characteristic, hyperbolic dependence upon the [ligand] reaching the plateau values at a higher [ligand]. Such

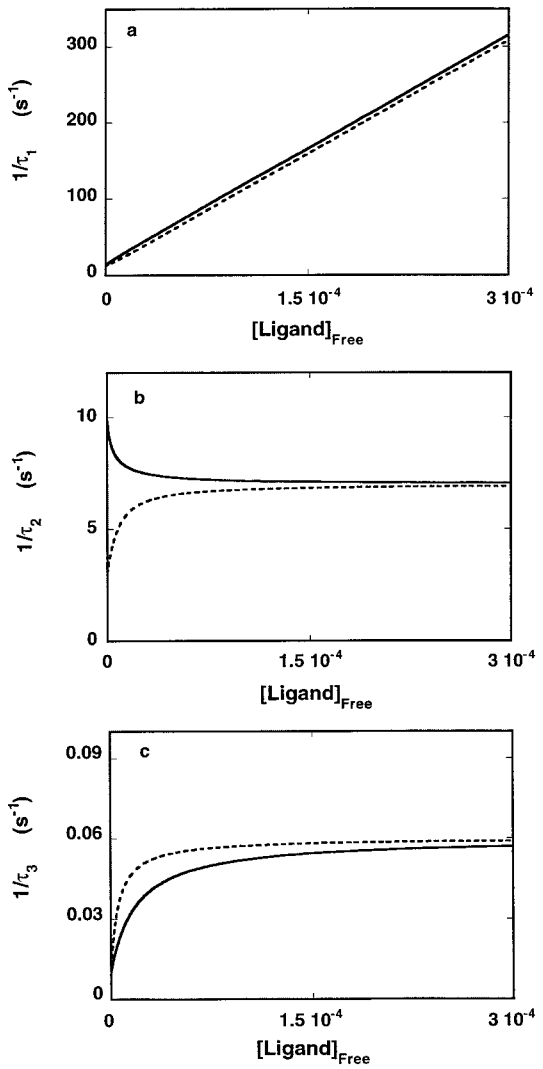

FIGURE 1: Computer simulation of the dependence of the reciprocal relaxation times for the mechanism of ligand binding to a macromolecule that undergoes a conformational transition prior to the ligand binding, followed by the two-step, sequential binding of the ligand to one of the macromolecule conformations (eq 2), upon the free ligand concentration. Relaxation times have been obtained by numerically determining the eigenvalues of the coefficient matrix $\mathbf{M_1}$ (λ_1, λ_2, λ_3) and then using identities $1/\tau_1 = -\lambda_1$, $1/\tau_2 = -\lambda_2$, and $1/\tau_3 = -\lambda_3$. The solid lines are simulations performed using rate constants $k_1 = 7\ s^{-1}$, $k_{-1} = 6\ s^{-1}$, $k_2 = 1 \times 10^6\ M^{-1}\ s^{-1}$, $k_{-2} = 10\ s^{-1}$, $k_3 = 0.05\ s^{-1}$, and $k_{-3} = 0.01\ s^{-1}$. The dashed lines are simulations performed using rate constants $k_1 = 7\ s^{-1}$, $k_{-1} = 6\ s^{-1}$, $k_2 = 1 \times 10^6\ M^{-1}\ s^{-1}$, $k_{-2} = 3\ s^{-1}$, $k_3 = 0.05\ s^{-1}$, and $k_{-3} = 0.01\ s^{-1}$. (a) $1/\tau_1$, (b) $1/\tau_2$, and (c) $1/\tau_3$.

functional dependence would strongly indicate that, contrary to the true mechanism of the reaction (eq 2) that includes macromolecule preequilibrium transition, an intramolecular transition following the ligand binding is observed. The value of k_{-2} has little effect on the functional behavior of the relaxation time $1/\tau_3$, i.e., it characterizes an intramolecular process in eq 2.

Pseudo-First-Order Conditions with Respect to the Macromolecule Concentration. The problem of determining the proper mechanism of the reaction described by eq 2 can be solved by the combined application of both pseudo-first-order conditions, with respect to the ligand and the macromolecule concentrations. This approach is based on the fact that, depending on the pseudo-first-order conditions applied, there is a fundamental difference in the extent of the effect of the ligand on the protein conformational equilibrium. In the case discussed above for the large excess of the ligand, the macromolecule shifts from a completely free state to an almost completely ligand saturated state. In the situation where the experiment is performed under pseudo-first-order conditions with respect to the macromolecule concentration, even at the initial concentrations, the degree of macromolecular saturation with the ligand is very low and decreases with the [macromolecule]. In other words, under pseudo-first-order conditions with respect to the macromolecule concentration, the ligand does not affect the internal equilibrium of the macromolecular conformational transition to any detectable extent. This has a profound, qualitative effect on the observed kinetics. As a result, the normal mode associated with the pre-equilibrium transition of the protein and the corresponding relaxation time becomes undetectable. What is experimentally observed is the intrinsic binding of the ligand to one of the macromolecule conformations, as described by

$$N + P_2 \underset{k_{-2}}{\overset{k_2}{\leftrightarrow}} P_3 \underset{k_{-3}}{\overset{k_3}{\leftrightarrow}} P_4 \tag{7}$$

The system of differential equations describing the time course of the reaction in eq 7 is a simple, two-step sequential binding mechanism that, in terms of the ligand species, is defined as

$$\begin{pmatrix} \dot{N} \\ \dot{P}_3 \\ \dot{P}_4 \end{pmatrix} = \begin{pmatrix} -k_2[P_2] & k_{-2} & 0 \\ k_2[P_2] & -(k_{-2} + k_3) & k_{-3} \\ 0 & k_3 & -k_{-3} \end{pmatrix} \begin{pmatrix} N \\ P_3 \\ P_4 \end{pmatrix} \tag{8}$$

and

$$\dot{\mathbf{N}} = \mathbf{M_2 N} \tag{9}$$

where $[P_2]$ can be expressed using the total protein concentration, P_{Tot}, as

$$[P_2] = \frac{P_{Tot} k_1}{k_{-1} + k_1} \tag{10}$$

The system of differential eqs 8 can be analytically solved. In terms of matrix projection operators, it is expressed as

$$\mathbf{N} = \mathbf{Q_0 N_0} + \mathbf{Q_1 N_0} \exp(\lambda_1 t) + \mathbf{Q_2 N_0} \exp(\lambda_2 t) \tag{11}$$

where the column vector of the initial concentrations of the ligand, $\mathbf{N_0}$, is defined as

$$\mathbf{N_0} = (N_{Tot} \quad 0 \quad 0) \tag{12}$$

Notice that in the case of a sequential reaction such a profound and easy to detect qualitative difference in the number of relaxation times between the two experimental conditions would never occur. Thus, for the sequential reaction, independent of whether the ligand or the macromolecule is in excess, the same number of relaxation times, i.e., the same number of normal modes of the reaction, will be always observed (*38*). Performing the kinetic studies in two different experimental environments, in pseudo-first-order conditions with respect to the ligand and to the

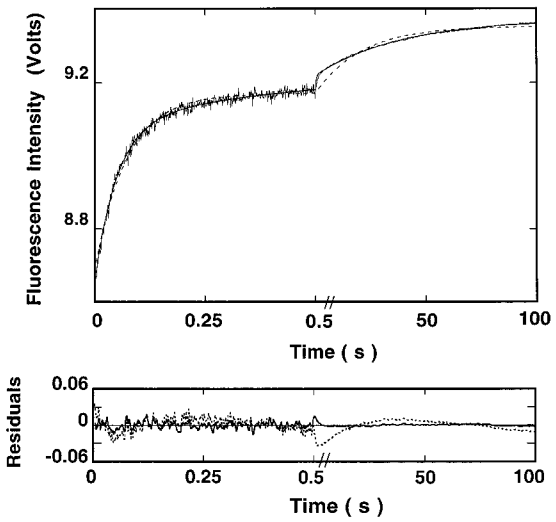

FIGURE 2: Fluorescence stopped-flow kinetic trace recorded in two time bases, 0.5 and 100 s, after mixing the DnaC with MANT-ATP in buffer T4 (pH 8.1, 20 °C), containing 100 mM NaCl (λ_{ex} = 356 nm, λ_{em} > 400 nm). The final concentrations of the DnaC and the nucleotide are 2×10^{-6} and 2.5×10^{-5} M, respectively. The solid line is the three-exponential nonlinear, least-squares fit of the experimental curve using eq 1. The dashed line is the two-exponential nonlinear, least-squares fit of the experimental trace using eq 1. The lower panel shows the residuals of the fit using the two-exponential (---) and three-exponential (—) functions, respectively.

macromolecule concentration, provides the experimenter with a crucial, empirical test for establishing the correct mechanism of the examined reaction.

RESULTS

Kinetic Mechanism of MANT-ATP Binding to the DnaC Protein. Binding of an unmodified nucleotide, ATP and ADP, to the DnaC protein is not accompanied by an adequate fluorescence change of the protein fluorescence (*27*). However, our previous studies have shown that binding of the fluorescent nucleotide analogues, MANT-ATP and MANT-ADP, is accompanied by a strong increase of the analogue fluorescence, thus, providing an excellent signal to monitor the complex kinetics. Moreover, the analogues have an affinity very similar to the unmodified nucleotides indicating that the MANT group does not affect the interactions with the protein (*27*).

In the first set of experiments, the kinetics of MANT-ATP binding to the DnaC protein has been performed under pseudo-first-order conditions with respect to the nucleotide concentration, i.e., the DnaC protein has been mixed in the stopped-flow instrument with a large excess of MANT-ATP. The stopped-flow trace of the MANT-ATP fluorescence, after mixing 2×10^{-6} M DnaC protein with 2.5×10^{-5} M nucleotide (final concentration) in buffer T4 (pH 8.1, 20 °C), containing 100 mM NaCl, is shown in Figure 2. The kinetic traces have been collected in two time bases, 0.5 and 100 s. The visual inspection of the curve already shows a complex multiexponential behavior confirmed by nonlinear, least-squares fit. The continuous line in Figure 2 is a nonlinear, least-squares fit of eq 1 to the experimental kinetic trace using a three-exponential fit. As indicated by the dashed line and included residuals, the two-exponential function does not

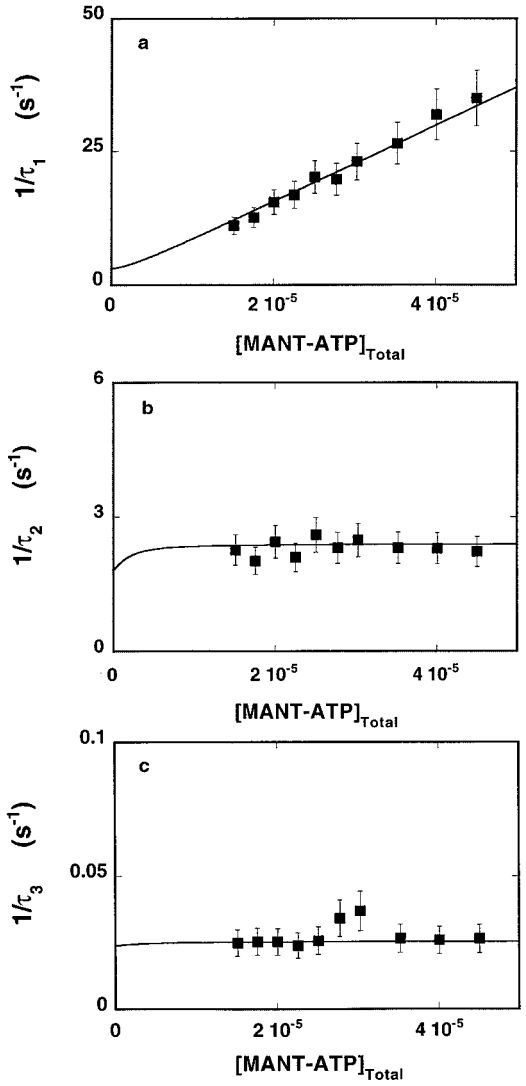

FIGURE 3: Dependence of the reciprocal of the relaxation times for the binding of MANT-ATP to the DnaC protein in buffer T4 (pH 8.1, 20 °C), containing 100 mM NaCl, upon the total concentration of the nucleotide. The concentration of the DnaC is 2×10^{-6} M. The solid lines are nonlinear, least-squares fits of the experimental data to the mechanism, defined by Scheme 1, using the rate constants $k_1 = 2.4\ s^{-1}$, $k_{-1} = 0.6\ s^{-1}$, $k_2 = 7.2 \times 10^5\ M^{-1}\ s^{-1}$, $k_{-2} = 1.8\ s^{-1}$, $k_3 = 0.0015\ s^{-1}$, and $k_{-3} = 0.024\ s^{-1}$ (Table 1). (a) $1/\tau_1$, (b) $1/\tau_2$, and (c) $1/\tau_3$. The error bars are standard deviations obtained from 3 to 4 independent experiments.

provide an adequate representation of the experimental curve. Moreover, a higher number of exponents does not significantly improve the statistics of the fit (data not shown). Thus, the obtained data indicate that under pseudo-first-order conditions with respect to [MANT-ATP], the binding of the nucleotide to the DnaC protein is a process that includes at least three steps.

The reciprocal relaxation times, $1/\tau_1$, $1/\tau_2$, and $1/\tau_3$, characterizing the three binding steps, as functions of the total MANT-ATP concentration, are shown in Figure 3a−c. The largest reciprocal time, $1/\tau_1$, increases with [MANT-ATP] in a linear fashion. Such behavior is typical for the relaxation time characterizing the bimolecular binding step (*36*−*41*). On the other hand, within experimental accuracy, both $1/\tau_2$ and $1/\tau_3$ show that they are independent of [MANT-ATP] in the examined nucleotide concentration range (see below).

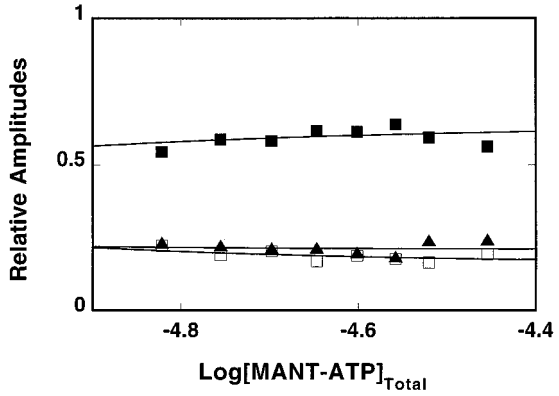

FIGURE 4: Dependence of the individual relaxation amplitudes of the kinetic process of MANT-ATP binding to the DnaC protein in buffer T4 (pH 8.1, 20 °C), containing 100 mM NaCl, upon the logarithm of the total concentration of the ATP analogue. The solid lines are computer fits according to the mechanism defined by Scheme 1, using eq A8 (Appendix 1), with the relative fluorescence intensities, $F_2 = 2.4$ and $F_3 = 8.64$. The fluorescence intensity of the free MANT-ATP is taken as $F_1 = 1$. The maximum fluorescence increase of the nucleotide has been determined in the equilibrium fluorescence titration as $\Delta F_{max} = 1.8$ (*27*). The rate constants are the same as those obtained from the relaxation time analysis (Figure 4, Table 1); A_1 (■), A_2 (□), and A_3 (▲).

Figure 4 shows the dependence of the individual amplitudes A_1, A_2, and A_3 for the three relaxation steps upon the logarithm of the total MANT-ATP concentration. The individual amplitudes are expressed as fractions of the total amplitude, $A_i/\sum A_i$. In the examined nucleotide concentration range, the amplitude A_1 of the first relaxation step slightly increases with the cofactor concentration and dominates the relaxation process. On the other hand, the value of the amplitude A_2 decreases with the increasing nucleotide concentration, while A_3 is independent of [MANT-ATP].

Such behavior of the relaxation times and amplitudes would strongly indicate that the mechanism of the ATP analogue binding to the DnaC protein is a sequential, three-step reaction, where the initial binding is followed by two isomerizations of the formed complex as (*38*)

$$N + P_1 \underset{k_{-1}}{\overset{k_1}{\leftrightarrow}} P_2 \underset{k_{-2}}{\overset{k_2}{\leftrightarrow}} P_3 \underset{k_{-3}}{\overset{k_3}{\leftrightarrow}} P_4 \qquad (13)$$

However, the examination of the same reaction under pseudo-first-order conditions, with respect to the protein concentrations, shows that this is not the case.

The stopped-flow trace of the MANT-ATP fluorescence, after mixing 5×10^{-7} M nucleotide with 1.74×10^{-5} M DnaC protein (final concentration) in buffer T4 (pH 8.1, 20 °C), containing 100 mM NaCl, is shown in Figure 5. The kinetic trace has been collected in two time bases, 1 and 200 s. The continuous line in Figure 5 is a nonlinear, least-squares fit of the experimental curve using a two-exponential fit. It is evident from included residuals that the two-exponential fit provides an excellent description of the experimental kinetic trace. A higher number of exponents does not significantly improve the statistics of the fit (data not shown). Thus, the same reaction that in the large excess of the nucleotide proceeds in three steps, under pseudo-first-order conditions with respect to the [DnaC], proceeds in only two steps (see above).

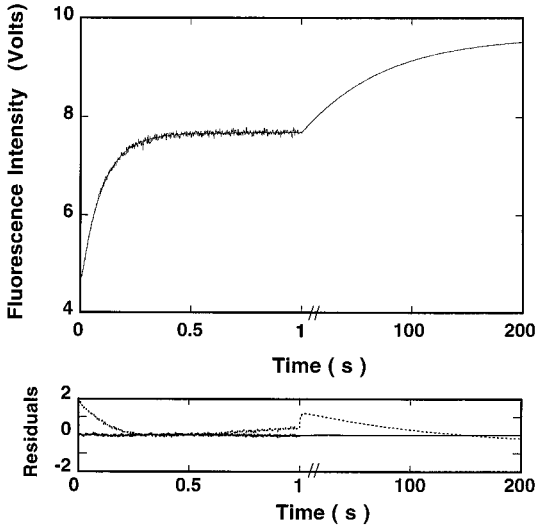

FIGURE 5: Fluorescence stopped-flow kinetic trace recorded in two time bases, 1 and 200 s, after mixing MANT-ATP with the DnaC protein in buffer T4 (pH 8.1, 20 °C), containing 100 mM NaCl, ($\lambda_{ex} = 356$ nm, $\lambda_{em} > 400$ nm). The final concentrations of the nucleotide and the protein are 5×10^{-7} and 1.74×10^{-5} M, respectively. The solid line is the two-exponential nonlinear, least-squares fit of the experimental curve using eq 1. The lower panel shows the residuals of the fit using the single-exponential (---) and two-exponential (—) functions, respectively.

The reciprocal relaxation times, $1/\tau_1$ and $1/\tau_2$, characterizing the two binding steps, as functions of the total DnaC concentration, are shown in Figure 6a,b. The corresponding relative amplitudes as functions of the logarithm of the total [DnaC] are shown in Figure 6c. The largest reciprocal relaxation time, $1/\tau_1$, linearly increases with [DnaC] and has, within experimental accuracy, the same values as the corresponding relaxation time obtained in the excess of the nucleotide (Figure 3a). The values of $1/\tau_2$ show independence of [MANT-ATP] and are the same as the values of $1/\tau_3$ in Figure 3c. Thus, the obtained data show that under pseudo-first-order conditions, with respect to the DnaC protein concentration, the intermediate relaxation time observed in the excess of the ligand is absent in the relaxation process. Such behavior excludes the sequential three-step process as the mechanism describing the kinetics of MANT-ATP binding to the DnaC protein. Moreover, in the context of our previous discussion (see above), it provides direct evidence of the presence of the conformational transition of the protein prior to the cofactor binding. Therefore, the minimum mechanism that describes MANT-ATP binding to the DnaC protein includes the conformational transition of the protein prior to the cofactor binding, followed by the two-step, sequential association of the nucleotide to one of the protein conformations defined by Scheme 1.

The determination of the rate constants of the particular steps and molar fluorescence parameters characterizing each intermediate requires the simultaneous analysis of both relaxation times and amplitudes. We applied the following strategy to obtain all rates and spectroscopic parameters of the system (*36*, *37*, *44*, *45*). First, the analysis was performed by numerically fitting the individual relaxation times. Here we utilized the fact that we know the value of the macroscopic or overall binding constant, $K_{MANT-ATP} = (3 \pm 0.4) \times 10^5\ M^{-1}$, independently obtained in the same solution conditions by the equilibrium fluores-

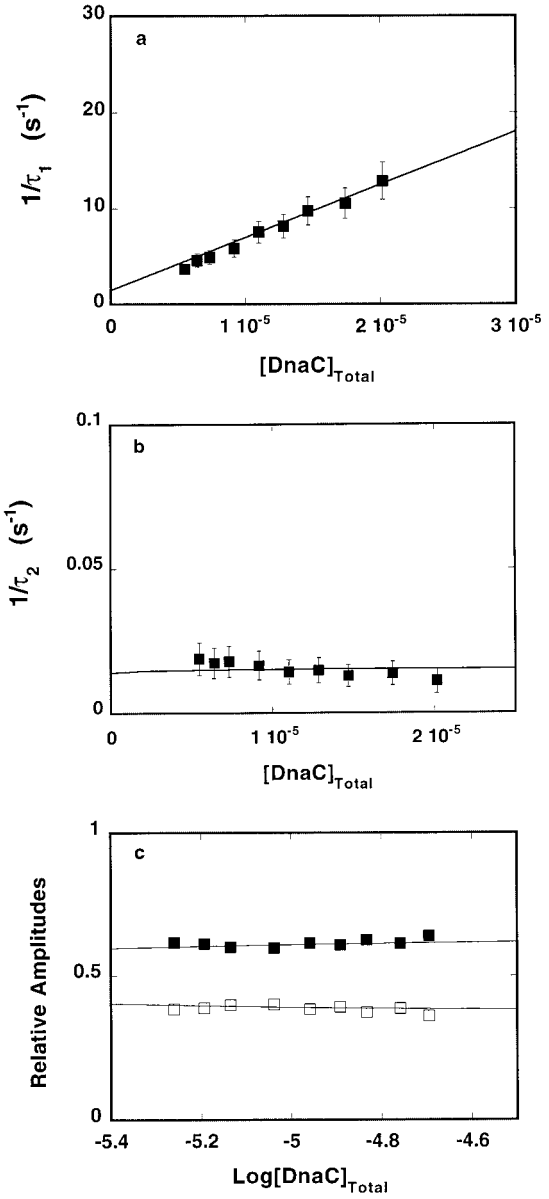

FIGURE 6: Dependence of the reciprocal of the relaxation times for the binding of MANT-ATP to the DnaC protein in buffer T4 (pH 8.1, 20 °C), containing 100 mM NaCl, upon the total concentration of the DnaC, i.e., the experiments have been performed under pseudo-first-order conditions with respect to the DnaC protein concentration. The concentration of MANT-ATP is 5×10^{-7} M. The solid lines are nonlinear, least-squares fits according to the mechanism, defined by Scheme 1, with the rate constants $k_1 = 2.4\ s^{-1}$, $k_{-1} = 0.6\ s^{-1}$, $k_2 = 6.9 \times 10^5\ M^{-1}\ s^{-1}$, $k_{-2} = 1.5\ s^{-1}$, $k_3 = 0.0015\ s^{-1}$, and $k_{-3} = 0.014\ s^{-1}$. (a) $1/\tau_1$ and (b) $1/\tau_2$. The error bars are standard deviations obtained from 3 to 4 independent experiments. (c) The dependence of the individual relaxation amplitudes of the kinetic process of MANT-ATP binding to the DnaC protein in buffer T4 (pH 8.1, 20 °C), containing 100 mM NaCl, upon the logarithm of the total DnaC concentration. The solid lines are computer fits according to the mechanism defined by Scheme 1, using eq A11 (Appendix 1), with the relative fluorescence intensities, $F_2 = 2.1$ and $F_3 = 9$. The fluorescence intensity of the free MANT-ATP is taken as $F_1 = 1$. The maximum fluorescence increase of the nucleotide has been determined in the equilibrium fluorescence titration as $\Delta F_{max} = 1.8$ (*27*). The rate constants are the same as those obtained from the relaxation time analysis (Figure 7a,b, Table 1); A_1 (■) and A_2 (□).

cence titration method (*27*). For the considered mechanism described by Scheme 1, $K_{MANT-ATP}$ is related to the partial

Scheme 1

$$(DnaC)_1 \underset{k_{-1}}{\overset{k_1}{\leftrightarrow}} (DnaC)_2$$

$$Nucleotide + (DnaC)_2 \underset{k_{-2}}{\overset{k_2}{\leftrightarrow}} (C)_1 \underset{k_{-3}}{\overset{k_3}{\leftrightarrow}} (C)_2$$

equilibrium steps by

$$K_{ATP} = \frac{K_1 K_2 (1 + K_3)}{1 + K_1} \tag{14}$$

where $K_1 = k_1/k_{-1}$, $K_2 = k_2/k_{-2}$, and $K_3 = k_3/k_{-3}$. Introducing the above relationship reduces to five the number of independent parameters in fitting the relaxation times.

The obtained rate constants were used as starting values in the fitting of the three individual amplitudes using the matrix projection operators technique described in Appendix 1. This method allows us to determine the molar fluorescence intensities characterizing each intermediate of the reaction, i.e., to assess the conformational state of the protein−nucleotide complex in each intermediate. The determination is facilitated by the fact that the maximum fractional increase of the MANT-ATP fluorescence, $\Delta F_{max} = 1.8 \pm 0.1$, is known from the equilibrium titrations (*27*). Moreover, ΔF_{max} can be analytically expressed as

$$\Delta F_{max} = \frac{\Delta F_2}{1 + K_3} + \frac{K_3 \Delta F_3}{1 + K_3} \tag{15}$$

where $\Delta F_2 = (F_2 - F_1)/F_1$ and $\Delta F_3 = (F_3 - F_1)/F_1$ are fractional fluorescence intensities of each intermediate in the association reaction of MANT-ATP with the DnaC protein, relative to the molar fluorescence intensity of the free nucleotide, F_1. Notice, contrary to the ΔF_i's, the fluorescence parameters F_2 and F_3 are relative molar fluorescence intensities, but not fractional intensities, with respect to the free nucleic acid fluorescence. Equation 15 provides an additional relationship between the fluorescence parameters. In the final step of the analysis, global fitting that simultaneously includes all relaxation times and amplitudes refines the values of the rate constants and molar fluorescence parameters.

The solid lines in Figures 3a−c and 4 are computer fits of the relaxation times and amplitudes according to the mechanism defined by Scheme 1, using a single set of the parameters. The obtained rate constants and relative molar fluorescence intensities are included in Table 1. Analysis of the relaxation times and amplitudes obtained under pseudo-first-order conditions with respect to the DnaC concentration has been analogously performed, using the same mechanism as that described by Scheme 1, with the concentration of P_2 defined by eq 10. The solid lines in Figure 6a−c are computer fits of the relaxation times and amplitudes using a single set of parameters (Table 1). As expected, both sets of data provide similar values of rate constants and relative molar fluorescence intensities of all intermediates.

The partial equilibrium constants for each step in Scheme 1 are $K_1 = k_1/k_{-1}$, $K_2 = k_2/k_{-2}$, and $K_3 = k_3/k_{-3}$. Introducing the values of the rate constants obtained under pseudo-first-order conditions, with respect to [MANT-ATP], provides $K_1 = 4 \pm 1.5$, $K_2 = (4 \pm 1.8) \times 10^5\ M^{-1}$, and $K_3 = 0.063 \pm 0.020$. The value of K_1 indicates that the equilibrium between

Table 1: Kinetic, Thermodynamic, and Spectroscopic Parameters Characterizing the Binding of MANT-ATP to the DnaC Protein in Buffer T4 (pH 8, 20 °C), Containing 100 MM NaCl, Obtained under Two Different Pseudo-First-Order Conditions

pseudo-first-order conditions	k_1 (s^{-1})	k_{-1} (s^{-1})	k_2 (s^{-1})	k_{-2} (s^{-1})	k_3 (s^{-1})	k_{-3} (s^{-1})	K_1	K_2 (M^{-1})	K_3	K_{ov}[a] (M^{-1})	F_2[b]	F_3[b]
MANT-ATP	2.4 ± 0.5	0.6 ± 0.1	$(7.2 \pm 1.5) \times 10^5$	1.8 ± 0.2	0.0015 ± 0.0005	0.024 ± 0.005	4 ± 1.5	$(4 \pm 1.8) \times 10^5$	0.063 ± 0.02	$(3 \pm 0.4) \times 10^5$	2.40 ± 0.11	8.64 ± 0.21
DnaC	2.4 ± 0.5	0.6 ± 0.1	$(6.9 \pm 1.4) \times 10^5$	1.5 ± 0.3	0.0015 ± 0.0005	0.014 ± 0.003	4 ± 1.5	$(4.6 \pm 1.5) \times 10^5$	0.107 ± 0.041	$(3 \pm 0.4) \times 10^5$	2.10 ± 0.12	9 ± 0.21

[a] The overall macroscopic binding constant, K_{ov}, has been determined in independent equilibrium titrations (*27*). [b] Values relative to the fluorescence, $F_1 = 1$ of the free MANT-ATP (details in text).

the two DnaC protein conformations, in absence of the nucleotide cofactor, is shifted toward the state that binds MANT-ATP. The bimolecular step makes a dominant contribution to the free energy of the nucleotide binding. Notice that the value of K_2 is larger than the value of the overall binding constant, $K = (3 \pm 0.4) \times 10^5$ M^{-1}, determined in independent fluorescence titrations (*27*). This results from the fact that part of the free energy of binding of the first step is used to shift the protein conformation toward the state that binds the nucleotide. The second binding step is energetically unfavorable.

MANT fluorescence is very sensitive to the polarity of the molecular environment (*31*, *47*). Amplitude analysis indicates only a moderate increase of the MANT-ATP emission accompanying the formation of the $(C)_1$ intermediate. This result suggests that in the first intermediate the MANT group is placed in a rather hydrophilic environment, possibly, still having access to the solvent (accompanying paper). However, a large increase of fluorescence intensity accompanying the $(C)_1 \leftrightarrow (C)_2$ transition provides a strong indication that the fluorophore is being shifted into a strong hydrophobic region of the binding site in $(C)_2$ with limited, if any, access to the solvent (accompanying paper).

Kinetic Mechanism of MANT-ADP Binding to the DnaC Protein. The analysis of the kinetic mechanism of MANT-ADP binding to the DnaC protein has been performed in an analogous way, as described for MANT-ATP. The experiments have been performed under pseudo-first-order conditions with respect to both the nucleotide and the protein concentrations. The obtained results show that under pseudo-first-order conditions with respect to [MANT-ADP], the kinetic traces required a three-exponential function (eq 1) to adequately represent the experimental curve indicating that binding of the nucleotide to the DnaC protein is a process that includes at least three steps (data not shown).

The reciprocal relaxation times, $1/\tau_1$, $1/\tau_2$, and $1/\tau_3$, characterizing the three binding steps, as functions of the total MANT-ADP concentration, are shown in Figure 7a–c. The behavior of the largest reciprocal time, $1/\tau_1$, is typical for the relaxation time characterizing the bimolecular binding step (*36*−*38*, see above). On the other hand, both $1/\tau_2$ and $1/\tau_3$ show independence of [MANT-ADP], suggesting that they characterize intramolecular transitions. The dependence of the corresponding relative individual amplitudes, A_1, A_2, and A_3, of all three relaxation steps upon the logarithm of the total MANT-ADP concentration is shown in Figure 8. As we pointed out, such behavior of the relaxation times and amplitudes could be interpreted as a sequential, three-step reaction (*36*,*37*). However, the relaxation process under pseudo-first-order conditions with respect to the protein concentration shows only two relaxation processes, as observed in the case of MANT-ATP (see above).

The reciprocal relaxation times $1/\tau_1$ and $1/\tau_2$ characterizing the two binding steps in the case of MANT-ADP, as functions of the total DnaC concentration, are shown in Figure 9a,b. The corresponding relative amplitudes as functions of the logarithm of the total [DnaC] are shown in Figure 9c. It is evident that under pseudo-first-order conditions, with respect to the DnaC protein concentration, the intermediate relaxation time observed in the excess of MANT-ADP is absent in the relaxation process. Such behavior excludes the three-step sequential process as the

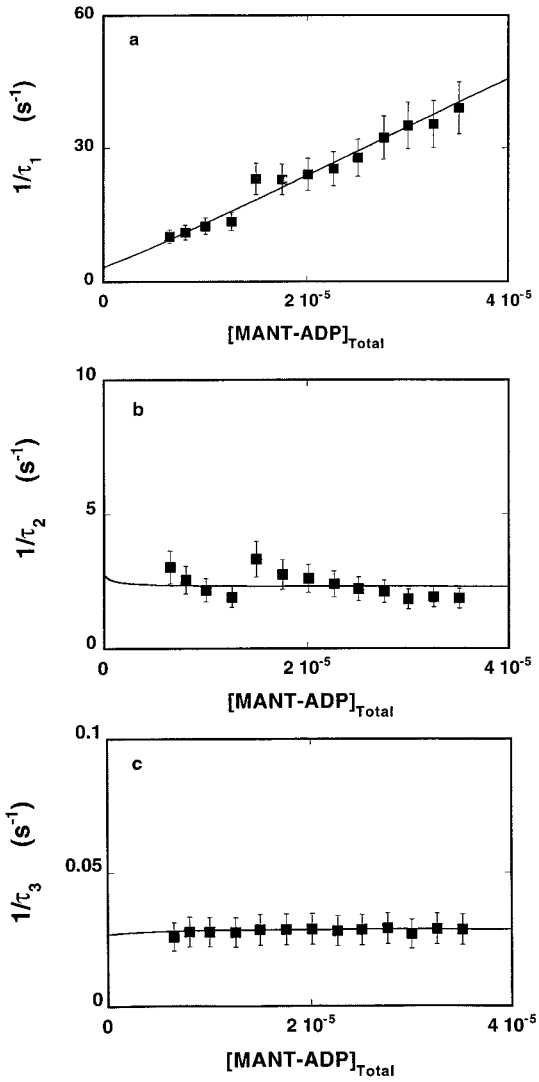

FIGURE 7: Dependence of the reciprocal of the relaxation times for the binding of MANT-ADP to the DnaC protein in buffer T4 (pH 8.1, 20 °C), containing 100 mM NaCl, upon the total concentration of the nucleotide, i.e., the experiments have been performed in pseudo-first-order conditions with respect to the nucleotide concentration. The concentration of DnaC protein is 2×10^{-6} M. The solid lines are nonlinear, least-squares fits of the experimental data to the mechanism, defined by Scheme 1, using the rate constants $k_1 = 2.4\ s^{-1}$, $k_{-1} = 0.6\ s^{-1}$, $k_2 = 1.1 \times 10^6\ M^{-1}\ s^{-1}$, $k_{-1} = 3\ s^{-1}$, $k_3 = 0.002\ s^{-1}$, and $k_{-3} = 0.027\ s^{-1}$ (Table 2). (a) $1/\tau_1$, (b) $1/\tau_2$, and (c) $1/\tau_3$. The error bars are standard deviations obtained from 3 to 4 independent experiments.

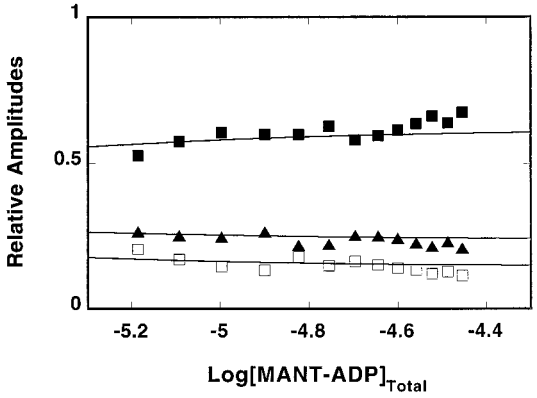

FIGURE 8: Dependence of the individual relaxation amplitudes of the kinetic process of MANT-ADP binding to the DnaC protein in buffer T4 (pH 8.1, 20 °C) containing 100 mM NaCl, upon the logarithm of the total concentration of the ADP analogue. The solid lines are computer fits according to the mechanism defined by Scheme 1, using eq A8 (Appendix 1), with the relative fluorescence intensities, $F_2 = 2.13$ and $F_3 = 7.25$. The fluorescence intensity of the free MANT-ADP is taken as $F_1 = 1$. The maximum fluorescence increase of the nucleotide has been determined in the equilibrium fluorescence titration as $\Delta F_{max} = 1.5$ (*27*). The rate constants are the same as those obtained from the relaxation time analysis (Figure 8, Table 2); A_1 (■), A_2 (□), and A_3 (▲).

mechanism describing the kinetics of MANT-ADP binding to the DnaC protein (see above). Thus, the minimum mechanism that describes MANT-ADP binding to the DnaC protein is the same as that determined for MANT-ATP and defined by Scheme 1. It includes the conformational transition of the DnaC protein, prior to cofactor binding, followed by the two-step, sequential association of the nucleotide to one of the protein conformations.

The analysis of the relaxation times and amplitudes to extract rate constants of particular steps and molar fluorescence parameters characterizing each intermediate has been performed in the same way as that described above for MANT-ATP. Here, we also utilize the fact that we know the value of the macroscopic binding constant, $K_{MANT-ADP} = (3 \pm 0.4) \times 10^5\ M^{-1}$, independently obtained in the same solution conditions by the equilibrium fluorescence titration method (*27*). $K_{MANT-ADP}$ is also defined in terms of equilibrium constants characterizing partial reactions by eq 14. Moreover, the amplitude analysis is facilitated by the fact that the maximum, fractional increase of the MANT-ADP fluorescence, $\Delta F_{max} = 1.5 \pm 0.1$, is known from the equilibrium titrations (*27*). Knowledge of the value of the K_{ADP} and ΔF_{max} reduces the number of independent parameters in the fitting procedures. The solid lines in Figures 7a−c and 8 are computer fits of the relaxation times and amplitudes, according to the mechanism defined by Scheme 1, using a single set of parameters. The solid lines in Figure 9 are computer fits using the single set of parameters obtained from the independent analysis of the kinetic mechanism defined by Scheme 1 under pseudo-first-order conditions with respect to the DnaC protein. Both sets of obtained rate constants and relative molar fluorescence intensities are included in Table 2.

Notice that the rate constants k_1 and k_{-1} are the same as those determined for MANT-ATP binding (Tables 1 and 2). This is expected because these parameters characterize the dynamics between the two protein conformations prior to the nucleotide binding. Also, the partial equilibrium constant $K_1 = 4 \pm 1.5$ is the same for both ATP and ADP analogues, which indicates that both nucleotide cofactors bind to the same conformation of the protein (see Discussion). As observed for the ATP analogue, the bimolecular step makes a dominant contribution to the free energy of the nucleotide binding. The value of K_2 is larger than the value of the overall binding constant, K, resulting from the fact that part of the free energy of binding of the first step is used to shift the protein conformation toward the state that binds the nucleotide. The second binding step is energetically unfavorable and is characterized by rate constants k_3 and k_{-3} which are very similar to the values of the same parameters obtained for MANT-ATP. Thus, the protein complexes with both nucleotide cofactors undergo a very similar transition following the binding step. Also, the amplitude analysis

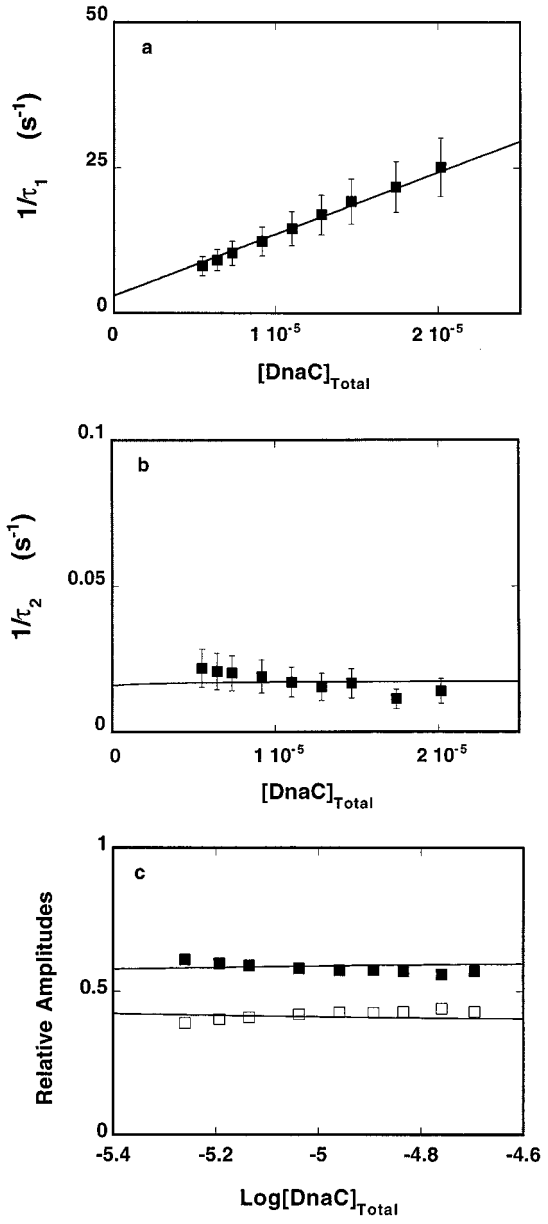

FIGURE 9: Dependence of the reciprocal of the relaxation times for the binding of MANT-ADP to the DnaC protein in buffer T4 (pH 8.1, 20 °C), containing 100 mM NaCl, upon the total concentration of the DnaC, i.e., the experiments have been performed under pseudo-first-order conditions, with respect to the DnaC protein concentration. The concentration of MANT-ADP is 5×10^{-7} M. The solid lines are nonlinear, least-squares fits according to the mechanism defined by Scheme 1, with the rate constants $k_1 = 2.4\ s^{-1}$, $k_{-1} = 0.6\ s^{-1}$, $k_2 = 1.33 \times 10^6\ M^{-1}\ s^{-1}$, $k_{-2} = 3\ s^{-1}$, $k_3 = 0.0016\ s^{-1}$, and $k_{-3} = 0.016\ s^{-1}$. (a) $1/\tau_1$ and (b) $1/\tau_2$. The error bars are standard deviations obtained from 3 to 4 independent experiments. (c) The dependence of the individual relaxation amplitudes of the kinetic process of MANT-ADP binding to the DnaC protein in buffer T4 (pH 8.1, 20 °C), containing 100 mM NaCl, upon the logarithm of the total DnaC concentration. The solid lines are computer fits according to the mechanism defined by Scheme 1, using eq A11 (Appendix 1) with the relative fluorescence intensities $F_2 = 1.91$ and $F_3 = 8.6$. The fluorescence intensity of the free MANT-ADP is taken as $F_1 = 1$. The maximum fluorescence increase of the nucleotide has been determined in the equilibrium fluorescence titration as $\Delta F_{max} = 1.5$ (*27*). The rate constants are the same as those obtained from the relaxation time analysis (Figure 10a,b, Table 2); A_1 (■) and A_2 (□).

Table 2: Kinetic, Thermodynamic, and Spectroscopic Parameters Characterizing the Binding of MANT-ADP to the DnaC Protein in Buffer T4 (pH 8, 20 °C), Containing 100 MM NaCl, Obtained under Two Different Pseudo-First-Order Conditions

pseudo-first-order conditions	k_1 (s^{-1})	k_{-1} (s^{-1})	k_2 (s^{-1})	k_{-2} (s^{-1})	k_3 (s^{-1})	k_{-3} (s^{-1})	K_1	K_2 (M^{-1})	K_3	K_{ov}[a] (M^{-1})	F_2[b]	F_3[b]
MANT-ADP	2.4 ± 0.5	0.6 ± 0.1	$(1.1 \pm 0.3) \times 10^6$	3 ± 0.3	0.002 ± 0.0005	0.027 ± 0.005	4.2 ± 1.8	$(3.7 \pm 1.5) \times 10^5$	0.074 ± 0.04	$(3 \pm 0.4) \times 10^5$	2.13 ± 0.11	7.25 ± 0.21
DnaC	2.4 ± 0.5	0.6 ± 0.1	$(1.33 \pm 0.3) \times 10^6$	3 ± 0.3	0.0016 ± 0.0004	0.016 ± 0.003	4 ± 1.8	$(4.4 \pm 1.8) \times 10^5$	0.1 ± 0.04	$(3 \pm 0.4) \times 10^5$	1.91 ± 0.11	8.6 ± 0.2

[a] The overall macroscopic binding constant, K_{ov}, has been determined in independent equilibrium titrations (*27*). [b] Values relative to the fluorescence, $F_1 = 1$ of the free MANT-ADP (details in text).

indicates that in the first intermediate, $(C)_1$, the molar fluorescence of MANT-ADP is increased only by a factor of ~ 2, similar to the value observed for the ATP analogue (Tables 1 and 2). However, the values of the relative molar fluorescence intensities of the final state, $(C)_2$, are systematically lower for MANT-ADP than for MANT-ATP, suggesting different orientations of the ribose region of both analogues in the $(C)_2$ intermediate.

DISCUSSION

DnaC Protein Exists in Two Different Conformations Prior to the Nucleotide Binding. Elucidation of the mechanism of interactions between nucleotide cofactors and the DnaC protein is of paramount importance for understanding the crucial role of the cofactors in regulating the physiological activities of the protein (*1*−*5*, *9*, *10*). The kinetic data and analyses described in this work provide direct evidence that the DnaC protein exists in equilibrium between two conformational states, $(DnaC)_1 \leftrightarrow (DnaC)_2$, prior to the nucleotide cofactor binding. Moreover, the obtained data indicate that the nucleotide only binds to one of the conformational states, $(DnaC)_2$. The fact that the $(DnaC)_1$ state is completely incapable of binding the nucleotide cofactors points to the existence of a very strict nucleotide binding site-locking mechanism. At present, it is unknown whether this mechanism of transforming the protein from a "closed" $(DnaC)_1$ to an "open" $(DnaC)_2$ conformation includes global conformational changes of the entire protein molecule or relies on the local structural changes around the binding site. Because, current data suggest that only the nucleotide-binding state of the DnaC protein binds to the DnaB helicase, it is most probable that allosteric changes of the protein structure include areas removed from the nucleotide binding site. Notice that the rate constants $k_1 = 2.4 \pm 0.5\ s^{-1}$ and $k_{-1} = 0.6 \pm 0.1\ s^{-1}$ characterizing the $(DnaC)_1 \leftrightarrow (DnaC)_2$ transition indicate that the structural change from the inactive to the active form of the protein occurs in a time range of hundreds of ms. Such a slow transition points to larger structural changes of the protein than just local opening and closing of the nucleotide-binding site. On the other hand, the value of the partial equilibrium constant, $K_1 = k_1/k_{-1} = 4 \pm 1.5$, characterizing the $(DnaC)_1 \leftrightarrow (DnaC)_2$ transition, indicates that the nucleotide binding state, $(DnaC)_2$, dominates the conformational distribution. As much as ~80% of the free DnaC protein molecules exist in the $(DnaC)_2$ state (see below). This result suggests that the DnaC system overpasses the slow conformational transition by keeping a large part of the protein molecule population in the nucleotide-binding state. Such overpass may be crucial for the fast response of the replication cycle of the *E. coli* cell, e.g., leading to a fast attachment to the DnaB helicase that is absolutely necessary for recognition of the origin of replication, oriC, by the helicase (*9*, *10*). The presence of a pre-equilibrium transition of the protein molecule, prior to its interaction with specific ligands, is a well-known phenomenon in various biological systems (*38*−*39*). Such an allosteric transition adds another level of regulation to the processes in which the protein is involved. The existence of ~20% of the protein molecule population in a state that is not capable of binding the nucleotide cofactor suggests that this DnaC protein state may play a role in the reactions where there is no stringent requirement for the nucleotide binding to the DnaC, e.g., in the formation of the primosome (*8*).

Two-Step Sequential Mechanism of the Intrinsic Nucleotide Binding to the "Open" Conformation of the DnaC Protein. The results obtained in this work indicate that the mechanism of MANT-ATP and MANT-ADP binding to the DnaC "open" conformational state, $(DnaC)_2$, is a minimum two-step, sequential process (see Scheme 1). Thus, the protein-nucleotide complex undergoes at least one conformational transition following the initial formation of the complex. The MANT moiety undergoes slow acyl-migration between the 2′ and 3′ OH group of the ribose that may affect the observed kinetics (*28*,*29*). On the basis of chemical studies, MANT-ATP and MANT-ADP were originally postulated to exist solely as 3′ isomers (*29*). However, NMR studies indicate that MANT-ATP and MANT-ADP exist as a mixture of 2′ and 3′ isomers, with the 3′ isomer being predominant (*47*). Our fluorescence lifetime and quantum yield analyses of various MANT analogues also indicate that the 3′ isomer is a predominant form of the nucleotide (*31*). Thermodynamic studies clearly show that the presence of the free 2′ OH group of the ribose is crucial for the nucleotide affinity for the DnaC protein (*27*). The affinities of dATP or dADP to the DnaC protein are by ~2−3 orders of magnitude weaker than affinities of corresponding ribose analogues. The overall affinity, $K_2 \times K_3$, of the $(C)_2$ intermediate is only by a factor of ~10−20 lower than the partial equilibrium constant, K_2, of the $(C)_1$ formation, arguing against a transition toward the 2′ isomer with 2−3 orders of magnitude lower affinity. Moreover, there is a very low fluorescence change of the MANT group accompanying the binding of MANT-dATP. This is contrary to the observed large fluorescence increase of the MANT moiety in the formation of the $(C)_2$ intermediate (Tables 1 and 2). Thus, it is rather unlikely that acyl migration of the MANT moiety between the 2′ and 3′ OH group of the ribose affects the observed kinetics, although this cannot be completely excluded. In other words, the data indicate that the two-step sequential mechanism of the nucleotide binding is an intrinsic property of the DnaC−nucleotide system (accompanying paper).

It should be noted that the highest value of the bimolecular association rate constant observed for MANT-ADP is $k_2 = (1.33 \pm 0.30) \times 10^6\ M^{-1}\ s^{-1}$, which is significantly lower than that expected for the diffusion-controlled reaction (*48*). Analysis analogous to the one previously described by us indicates that the diffusion-controlled association rate constant for the nucleotide−DnaC protein system is $k_D \sim 5 \times 10^9\ M^{-1}\ s^{-1}$ (*37*). Smaller interaction radii, or the presence of some orientation factors, could lower this value by a factor of ~100 to $k_D \sim 5 \times 10^7\ M^{-1}\ s^{-1}$, a value which is similar to that observed for some fast formations of the nucleotide cofactor−protein complexes (*49*). These values indicate that the determined bimolecular rate constant, k_2, is ~2−4 orders of magnitude lower than the k_D predicted by the diffusion-controlled collision, suggesting that the bimolecular association step contains an additional conformational transition of the DnaC−nucleotide complex.

Strong evidence for the presence of the additional transition following the collision complex comes from the amplitude analysis which indicates that an increase of the nucleotide fluorescence (possible conformational change of the protein−nucleotide complex) occurs in the formation of

Scheme 2

$$(\mathrm{DnaC})_1 \underset{k_{-1}}{\overset{k_1}{\leftrightarrow}} (\mathrm{DnaC})_2$$

$$\text{Nucleotide} + (\mathrm{DnaC})_2 \underset{k_{-D}}{\overset{k_D}{\leftrightarrow}} \mathrm{E} \underset{k'_{-2}}{\overset{k'_2}{\leftrightarrow}} (\mathrm{C})_1 \underset{k_{-3}}{\overset{k_3}{\leftrightarrow}} (\mathrm{C})_2$$

the $(C)_1$ intermediate (Tables 1 and 2). Such conformational changes of the DnaC−nucleotide complex cannot result from a simple collision (*48*). Therefore, Scheme 1 should be enlarged by an extra step following the collision complex, as described by Scheme 2, where k_D and k_{-D} are rate constants for the formation and dissociation of the collision complex and k'_2 and k'_{-2} are the rate constants for the transition from the collision complex to $(C)_1$. It should be pointed out that we do not observe an amplitude loss in the dead time of the instrument (∼2 ms), an indication that the collision process and the E ↔ $(C)_1$ transition are very fast, with no fluorescence change accompanying the E formation.

The estimate of the range of values for k'_2 can be obtained as follows. Notice that the dependence of the reciprocal relaxation time for the bimolecular process, $1/\tau_1$, for both MANT-ATP and MANT-ADP is a linear function of the nucleotide concentration at the highest concentrations examined (∼5×10^{-5} M). In the context of the Scheme 2, the value of $1/\tau_1$ should reach plateau at very high nucleotide concentration. The linear dependence results from the fact that the process is observed only in the limited, experimentally available nucleotide concentration range. The obtained data indicate that K_D must be lower than ∼2×10^4 M^{-1} (*36*). Taking a conservative value, $K_D \sim 10^3$ M^{-1} gives k'_2 ∼ 1000 s^{-1} for both nucleotide analogues. Thus, the obtained data strongly suggest that the collision complex, E, undergoes a transition to $(C)_1$ with a forward rate constant of more than ∼2 orders of magnitude larger than the dissociation constant, k_{-2}.

Both ATP and ADP Bind with the Same Mechanism to the Same DnaC Conformation. Recent thermodynamic studies showed that MANT-ATP and MANT-ADP, as well as unmodified nucleotides ATP and ADP, bind the DnaC protein with the same affinities (*27*). Kinetic analyses described in this work show that binding of the MANT-ATP and MANT-ADP proceeds with the same kinetic mechanism. Comparison between the data included in Tables 1 and 2 shows that rate constants characterizing partial steps, as well as the relative molar fluorescence intensities of the intermediates, are similar for both analogues. Thus, the presence of the extra phosphate group has no affect on the mechanism or the dynamics of the partial steps. Moreover, the values of rate constants k_1 and k_{-1} as well as the value of the equilibrium constant K_1 that characterize the conformational transition of the protein are, within experimental accuracy, the same for both analogues (Tables 1 and 2). As we pointed out above, this means that both analogues bind to the same $(DnaC)_2$ state of the protein. This is because if, e.g., MANT-ADP binds to the $(DnaC)_1$ state, then the forward rate constant would correspond to the determined backward rate constant, k_{-1}, and vice versa. In such a case, the value of K_1 would be $k_{-1}/k_1 \sim 0.25$, but this is not experimentally observed.

These results are rather surprising. Recall that only binding of ATP to the DnaC protein, not ADP, has been proposed to be specifically required for the formation of a stable DnaB helicase−DnaC protein complex (*9*, *10*). This difference in affecting the physiological functioning of the protein strongly suggests a large difference in the protein conformational states when bound to ATP or ADP. Our data indicate that either the DnaC complexes with ATP and ADP bind the DnaB helicase with the same affinity or else the differences in the protein structure in these complexes are subtle and do not affect the thermodynamics and kinetics of the nucleotide cofactor binding. Nevertheless, the relative molar fluorescence intensities characterizing the $(C)_1$ and $(C)_2$ intermediates are systematically higher for the ATP analogue, as compared with MANT-ADP (Tables 1 and 2). Such differences indicate that despite very similar dynamics and energetics of partial steps, the orientation of the MANT group, i.e., the orientation of the bound cofactor is different for ATP as compared to ADP.

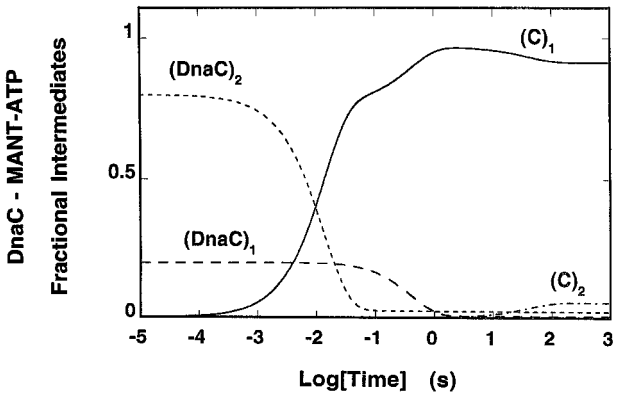

FIGURE 10: Computer simulation of the time course of the fractional concentration distribution of different DnaC protein species in the binding of MANT-ATP using the determined rate constants $k_1 = 2.4$ s^{-1}, $k_{-1} = 0.6s^{-1}$, $k_2 = 7.2 \times 10^5$ M^{-1} s^{-1}, $k_{-2} = 1.8$ s^{-1}, $k_3 = 0.0015$ s^{-1}, and $k_{-3} = 0.024$ s^{-1} (buffer T4 (pH 8.1, 20 °C), containing 100 mM NaCl). The total DnaC and nucleotide concentrations are 2×10^{-6} and 5×10^{-5} M, respectively. $(DnaC)_1$ (⁻·⁻), $(DnaC)_2$ (---), $(C)_1$ (—), $(C)_2$ (— - —).

It is interesting that the formation of the second intermediate, $(C)_2$, is an energetically unfavorable step ($K_3 \ll 1$). Moreover, the formation of the $(C)_2$ intermediate is a very slow reaction that requires minutes for completion (Tables 1 and 2). The time dependence of the distribution of the different DnaC species, in the presence of MANT-ATP, is shown in Figure 10. The plots have been generated using the parameters included in Table 1 for pseudo-first-order conditions, with respect to the nucleotide concentration. At equilibrium, $(C)_1$ constitutes ∼95% of the total protein population. Such fast formation and equilibrium predominance of the $(C)_1$ intermediate makes it the most probable substrate for the interaction with the DnaB helicase. Our laboratory is currently examining these interactions.

ACKNOWLEDGMENT

We wish to thank Gloria Drennan Bellard for her help in preparing the manuscript.

APPENDIX 1

Closed-Form Formulas for the Relaxation Amplitudes in Stopped-Flow Kinetics. In spectroscopic stopped-flow experiments, concentrations of the reactants and products are

indirectly monitored through some spectroscopic parameter (e.g., fluorescence) characterizing interacting species. In general, each intermediate will have different fluorescence properties. In the mechanism examined in this work (eq 2), there are three molar fluorescence intensities F_1, F_2, and F_3 characterizing the N_1, P_3, and P_4 states of the ligand, free and in the complex with the protein. Although the mechanism described by Scheme 1 cannot be analytically solved, application of the matrix projection operators reduces the numerical analysis of the multistep reaction to finding only the eigenvalues of the original coefficient matrix **M** which correspond to the relaxation times of the normal modes of reaction (*36*, *37*, *43*−*45*). The closed-form formulas for the amplitudes of the different normal modes of the reaction are obtained in terms of the relaxation times (eigenvalues) and the spectroscopic properties of each intermediate.

For the experiments conducted under pseudo-first-order conditions with respect to the fluorescent ligand concentration, the products of $\mathbf{Q_i P_0}$, eq 5 (see text), are column vectors, $\mathbf{R_i}$, that are the projections of the vector of the initial concentrations, $\mathbf{P_0}$, on each eigenvector of the coefficient matrix $\mathbf{M_1}$. Thus, the solution of system 3 is then

$$\mathbf{P} = \mathbf{R_0} + \mathbf{R_1}\exp(\lambda_1 t) + \mathbf{R_2}\exp(\lambda_2 t) + \mathbf{R_3}\exp(\lambda_3 t) \quad \text{(A1)}$$

and

$$\begin{pmatrix} P_1 \\ P_2 \\ P_3 \\ P_4 \end{pmatrix} = \begin{pmatrix} R_{01} \\ R_{02} \\ R_{03} \\ R_{04} \end{pmatrix} + \begin{pmatrix} R_{11} \\ R_{12} \\ R_{13} \\ R_{14} \end{pmatrix}\exp(\lambda_1 t) + \begin{pmatrix} R_{21} \\ R_{22} \\ R_{23} \\ R_{24} \end{pmatrix}\exp(\lambda_2 t) + \begin{pmatrix} R_{31} \\ R_{32} \\ R_{33} \\ R_{34} \end{pmatrix}\exp(\lambda_3 t) \quad \text{(A2)}$$

where R_{ij} is the jth element of the projection of $\mathbf{P_0}$ on the eigenvector corresponding to the ith eigenvalue of matrix $\mathbf{M_1}$.

The three normal modes of reaction characterized by amplitudes A_1, A_2, and A_3 have corresponding relaxation times $\tau_1 = -1/\lambda_1$, $\tau_2 = -1/\lambda_2$, and $\tau_3 = -1/\lambda_3$. The concentrations of all ligand species, at any time of the reaction, follow the mass conservation relationship

$$N_{\text{Tot}} = N_1 + P_3 + P_4 \quad \text{(A3)}$$

where P_3 and P_4 are defined by eq A2. The fluorescence of the system at time t of the reaction, $F(t)$, is defined by

$$F(t) = F_1 N_1 + F_2 P_3 + F_3 P_4 \quad \text{(A4)}$$

The observed total amplitude, A_{Tot}, of the stopped-flow trace is the sum of the individual amplitudes of all normal modes

$$A_{\text{Tot}} = A_1 + A_2 + A_3 \quad \text{(A5)}$$

Experimentally, for any stopped-flow trace, the amplitude, A_{Tot}, is described by

$$A_{\text{Tot}} = F(\infty) - F(0) \quad \text{(A6)}$$

where $F(\infty)$ and $F(0)$ are the observed fluorescence intensities, $F(t)$, of the system at $t = 0$ and $t = \infty$, respectively. Introducing the mass conservation relationship defined by eq A3 into eq A4, $t = 0$ for $F(0)$ and $t = \infty$ for $F(\infty)$, one obtains (*36*, *37*, *43*−*45*)

$$A_{\text{Tot}} = (R_{13} + R_{23} + R_{33} \quad R_{14} + R_{24} + R_{34})\begin{pmatrix} F_1 - F_2 \\ F_1 - F_3 \end{pmatrix} \quad \text{(A7)}$$

The individual amplitudes A_1, A_2, and A_3 for each normal mode are then

$$A_1 = (R_{13} \quad R_{14})\begin{pmatrix} F_1 - F_2 \\ F_1 - F_3 \end{pmatrix} \quad \text{(A8a)}$$

$$A_2 = (R_{23} \quad R_{24})\begin{pmatrix} F_1 - F_2 \\ F_1 - F_3 \end{pmatrix} \quad \text{(A8b)}$$

$$A_3 = (R_{33} \quad R_{34})\begin{pmatrix} F_1 - F_2 \\ F_1 - F_3 \end{pmatrix} \quad \text{(A8c)}$$

Equations A7, A8a, A8b, and A8c are closed-form, explicit expressions for the total and individual amplitudes for the observed, three-step reaction mechanism, described by eq 2, when the stopped-flow experiments are conducted under pseudo-first-order conditions with respect to the fluorescing ligand concentration.

For the stopped-flow experiments conducted under pseudo-first-order conditions with respect to the protein concentration, the observed relaxation process reduces to eq 8, and the solution of the system of differential eqs 9 can be analytically solved. In terms of matrix projection operators, it is defined by

$$\mathbf{P} = \mathbf{S_0} + \mathbf{S_1}\exp(\lambda_1 t) + \mathbf{S_2}\exp(\lambda_2 t) \quad \text{(A9)}$$

where the column vectors, $\mathbf{S_i}$, are the products $\mathbf{Q_i N_0}$ in eq 11 (see text) which are the projections of $\mathbf{N_0}$ on each eigenvector of the coefficient matrix, $\mathbf{M_2}$, providing

$$\begin{pmatrix} N_1 \\ P_3 \\ P_4 \end{pmatrix} = \begin{pmatrix} S_{01} \\ S_{02} \\ S_{03} \end{pmatrix} + \begin{pmatrix} S_{11} \\ S_{12} \\ S_{13} \end{pmatrix}\exp(\lambda_1 t) + \begin{pmatrix} S_{21} \\ S_{22} \\ S_{23} \end{pmatrix}\exp(\lambda_2 t) \quad \text{(A10)}$$

Analogous analysis as described above provides the total and individual amplitudes as

$$A_{\text{Tot}} = (S_{12} + S_{22} \quad S_{13} + S_{23})\begin{pmatrix} F_1 - F_2 \\ F_1 - F_3 \end{pmatrix} \quad \text{(A11a)}$$

and

$$A_1 = (S_{12} \quad S_{13})\begin{pmatrix} F_1 - F_2 \\ F_1 - F_3 \end{pmatrix} \quad \text{(A11b)}$$

$$A_2 = (S_{22} \quad S_{23})\begin{pmatrix} F_1 - F_2 \\ F_1 - F_3 \end{pmatrix} \quad \text{(A11c)}$$

REFERENCES

1. Kornberg, A., and Baker, T. A. (1992) *DNA Replication*, Freeman, San Francisco.
2. Marians, K. J. (1992) *Annu. Rev. Biochem. 61*, 673−719.
3. Skarstad, K., and Wold, S. (1995) *Mol. Microbiol. 17*, 825−831.
4. Wickner, S., Wright, M., and Hurwitz, J. (1973) *Proc. Natl. Acad. Sci. U.S.A. 71*, 783−787.

5. Wickner, S., and Hurwitz, J. (1974) *Proc. Natl. Acad. Sci. U.S.A. 72*, 921−925.
6. Wechsler, J. (1975) *J. Bacteriol. 121*, 594−599.
7. Wechsler, J., and Gross, J. D. (1971) *Mol. Gen. Genet. 113*, 273−284.
8. Marians, K. J. (1999) *Prog. Nucl. Acid. Res. Mol. Biol. 63*, 39−67.
9. Wahle, E., Lasken, R. S., and Kornberg, A. (1989a) *J. Biol. Chem. 264*, 2463−2468.
10. Wahle, E., Lasken, R. S., and Kornberg, A. (1989b) *J. Biol. Chem. 264*, 2469−2475.
11. Allen, G. C., and Kornberg, A. (1991) *J. Biol. Chem. 266*, 22096−22101.
12. Allen, G. C., and Kornberg, A. (1991) *J. Biol. Chem. 268*, 19204−19209.
13. Kobori, J. A., and Kornberg, A. (1982) *J. Biol. Chem. 257*, 13757−13762.
14. Kobori, J. A., and Kornberg, A. (1982) *J. Biol. Chem. 257*, 13763−13769.
15. Masai, H., and Arai, K. (1995) *Eur. J. Biochem. 230*, 384−395.
16. Bujalowski, W., and Jezewska, M. J. (1995) *Biochemistry 34*, 8513−8519.
17. Jezewska, M. J., and Bujalowski, W. (1996) *Biochemistry 35*, 2117−2128.
18. Jezewska, M. J., Kim, U.-S., and Bujalowski, W. (1996) *Biochemistry 36*, 2129−2145.
19. Jezewska, M. J., Rajendran S., Bujalowska, D., and Bujalowski, W. (1998) *J. Biol. Chem. 273*, 10515−10529.
20. Jezewska, M. J., Rajendran S., and Bujalowski, W. (1998) *J. Biol. Chem. 273*, 9058−9069.
21. Jezewska, M. J., Rajendran, S., and Bujalowski, W. (1997) *Biochemistry 36*, 10320−10326.
22. Sancar, A., and Hearst, J. E. (1993) *Science 259*, 1415−1420.
23. Nakayama, N., Arai, N., Bond, M. W., Miyajima, A., Kobori, J., and Arai, K. (1987) *J. Biol. Chem. 262*, 10475−10480.
24. Kobori, J. A., and Kornberg, A. (1982) *J. Biol. Chem. 257*, 13770−13775.
25. Lanka E., Geschke, B., and Schuster, H. (1978) *Proc. Natl. Acad. Sci. U.S.A. 75*, 799−803.
26. Lanka, E., and Schuster, H. (1983) *Nucl. Acid Res. 11*, 987−997.
27. Galletto, R., Rajendran, S., and Bujalowski, W. (2000) *Biochemistry 39*, 12959−12969
28. Hiratsuka, T., and Uchida, K. (1973) *Biochim. Biophys. Acta 320*, 635−647.
29. Hiratsuka, T. (1983) *Biochim. Biophys. Acta 742*, 496−508.
30. Bujalowski, W., and Klonowska, M. M. (1993) *Biochemistry 32*, 5888−5900.
31. Bujalowski, W., and Klonowska, M. M. (1994) *Biochemistry 33*, 4682−4694.
32. . Bujalowski, W., and Klonowska, M. M. (1994) *J. Biol. Chem.* 269 , 31359−31371.
33. Jezewska, M., J., Kim, U.-S., and Bujalowski, W. (1997) *Biophys. J. 71*, 2075−2086.
34. Lakowicz, J. R. (1999) *Principle of Fluorescence Spectroscopy*, Plenum Press, New York.
35. Otto, R., Lillo, M. P., and Beechem, J. M. (1994) *Biophys. J. 67*, 2511−2521.
36. Bujalowski, W., and Jezewska, M. J. (2000) *J. Mol. Biol. 295*, 831−852.
37. Bujalowski, W., and Jezewska, M. J. (2000) *Biochemistry 39*, 2106−2122.
38. Bernasconi, C. J. (1976) *Relaxation Kinetics*, Chapters 3−10, Academic Press, New York.
39. Eigen, M. (1968) *Q. Rev. Biophys. I*, 3−33.
40. Hammes, G. G., and Wu, K. (1974) *Annu. Rev. Biophys. Bioengin. 3*, 1−33.
41. Fierke, C. A., and Hammes, G. G. (1995) *Methods Enzymol. 249*, 3−37.
42. Bujalowski, W., Jung, M., McLaughlin, L. W., and Porschke, D. (1986) *Biochemistry 25*, 6372−6378.
43. Rajendran, S., Jezewska, M. J., and Bujalowski, W. (2000) *J. Mol. Biol. 303*, 773−795.
44. Rajendran, S., Jezewska, M. J., and Bujalowski, W (2001) *Biochemistry 40*, 11794−11810.
45. Jezewska, M. J., Rajendran, S., and Bujalowski, W (2001) *J. Mol. Biol. 313*, 977−1002.
46. Pilar, R. L. (1968) *Elementary Quantum Chemistry*, Chapter 9, McGraw-Hill, New York.
47. Cremo, C., R., Neuron, J. M., and Yount, R. G. (1990) *Biochemistry 29*, 3309−3319.
48. Connors, K. W. (1990) *Chemical Kinetics. The Study of Reaction Rates in Solution*, Chapter 4, pp 133−186, VCH, New York.
49. Hammes, G. G., and Schimmel, P. R. (1970) *The Enzymes. Kinetics and Mechanism*, Vol. II, Chapter 2, Academic Press, New York.

BI0201264